Structural Insights into Active Catalyst Structures and Oxidative Addition to (Biaryl)phosphine−Palladium Complexes via Density Functional Theory and Experimental Studies

Timothy E. Barder,* Mark R. Biscoe, and Stephen L. Buchwald*

Department of Chemistry, Massachusetts Institute of Technology, 77 Massachusetts Avenue, Cambridge, Massachusetts 02139

Received February 2, 2007

We present results on the structure of monoligated active catalysts based upon 2-dicyclohexylphosphino-2′,6′-dimethoxybiphenyl (SPhos, **1**) and 2-dicyclohexylphosphino-2′,4′,6′-triisopropylbiphenyl (XPhos, **2**) with Pd(0). Additionally, the reaction of SPhos·Pd with chlorobenzene has been explored via *all-atom* density functional theory (DFT) and these results are supported by NMR studies. The same reaction, but with a catalyst based on a larger ligand, XPhos·Pd, is also analyzed. Finally, it has been determined that inclusion of the entire ligand structure in these types of calculations is of importance for obtaining accurate and significant results.

In the past 20 years, the use of group 10 metals, particularly palladium, has seen enormous growth in the field of homogeneous catalysis.[1] This increased interest has resulted in a better understanding of these metals and their associated complexes, which has led to more intricately designed ligands. Oftentimes, catalysts consisting of "rationally designed" ligands possess characteristics not fully intended. However, numerous catalysts have permitted the use of much milder reaction conditions (e.g., low temperature, mild reagents, short reaction time, and nontoxic solvents) to promote difficult cross-coupling and other metal-catalyzed reactions that were impossible even 10 years ago.[1b,c] In order to expedite the development of more efficient catalyst systems, it is paramount to determine which structural characteristics of a ligand are most influential in promoting the formation of highly reactive and stable catalysts. Our group and others have reported X-ray crystal structures of ligated palladium complexes that possess Pd−arene interactions.[2] These types of interactions are believed to provide stability in the palladium complex and to increase the electron density at the palladium center, which may enhance the reactivity in certain steps within a catalytic cycle. However, there are limited data regarding the structure of monoligated phosphine−Pd complexes that lay within a catalytic cycle and the role of Pd−arene interactions in these types of complexes. Unfortunately, all previous attempts to structurally characterize monoligated arylpalladium complexes that contain a (biaryl)phosphine ligand and lay within a cross-coupling catalytic cycle have been unsuccessful.[3] However, as we feel that the knowledge derived from such studies is of great importance in understanding the catalytic cycle and creating more efficient and stable catalysts, we turned to computational chemistry to conduct structural analyses of various Pd(0) and Pd(II) complexes, that may lay within a catalytic cycle, with 2-dicyclohexylphosphino-2′,6′-dimethoxybiphenol (SPhos, **1**)[2d,f] and 2-dicyclohexylphosphino-2′,4′,6′-triisopropylbiphenyl (XPhos, **2**).[4] It is important to note that although **1** is most often utilized in Suzuki−Miyaura coupling reactions and **2** in amination reactions, either ligand can generate catalysts effective for both of these cross-coupling processes. Herein, we report possible structures for the active catalyst, transition-state structures of oxidative addition with chlorobenzene, and experimental and theoretical structures of oxidative addition intermediates based upon **1**·Pd and **2**·Pd.

Computational Methods

All calculations were conducted on a home-built Linux cluster consisting of 24 Xeon processors. Ground-state geometry optimizations, using all-atom DFT without any approximations, were conducted using Gaussian 03[5] with the B3LYP hybrid functional.[6] For C, H, and O, the 6-31G basis set was used, for P and Cl the

* To whom correspondence should be addressed. E-mail: tbarder@mit.edu (T.E.B.), sbuchwal@mit.edu (S.L.B.).

(1) (a) Negishi, E. *Acc. Chem. Res.* **1982**, *15*, 340−348. (b) Negishi, E., de Meijere, A., Eds. *Handbook of Organopalladium Chemistry for Organic Synthesis*; Wiley-Interscience: New York, 2002. (c) Tsuji, J. *Palladium Reagents and Catalysts*: *New Perspectives for the 21st Century*; Wiley: Chichester, West Sussex, England, 2004.

(2) (a) Kočovský, P.; Vyskočil, S.; Císařová, I.; Sejbal, J.; Tišlerová, I.; Smrčina, M.; Lloyd-Jones, G. C.; Stephen, S. C.; Butts, C. P.; Murray, M.; Langer, V. *J. Am. Chem. Soc.* **1999**, *121*, 7714−7715. (b) Yin, J.; Rainka, M. P.; Zhang, X.-X.; Buchwald, S. L. *J. Am. Chem. Soc.* **2002**, *124*, 1162−1163. (c) Dotta, P.; Kumar, P. G. A.; Pregosin, P. S.; Albinati, A.; Rizzato, S. *Organometallics* **2003**, *22*, 5345−5349. (d) Wang, Y.; Li, X.; Sun, J.; Ding, K. L. *Organometallics* **2003**, *22*, 1856−1862. (e) Reid, S. M.; Boyle, R. C.; Mague, J. T.; Fink, M. J. *J. Am. Chem. Soc.* **2003**, *125*, 7816−7817. (f) Faller, J. W.; Sarantopoulos, N. *Organometallics* **2004**, *23*, 2008−2014. (g) Dotta, P.; Kumar, P. G. A.; Pregosin, P. S.; Albinati, A.; Rizzato, S. *Organometallics* **2004**, *23*, 4247−4254. (h) Walker, S. D.; Barder, T. E.; Martinelli, J. R.; Buchwald, S. L. *Angew. Chem., Int. Ed.* **2004**, *43*, 1871−1876. (i) Christmann, U.; Vilar, R.; White, A. J. P.; Williams, D. J. *Chem. Commun.* **2004**, 1294−1295. (j) Barder, T. E.; Walker, S. D.; Martinelli, J. R.; Buchwald, S. L. *J. Am. Chem. Soc.* **2005**, *127*, 4685−4696. (k) Barder, T. E. *J. Am. Chem. Soc.* **2006**, *128*, 898−904. (l) Christmann, U.; Pantazis, D. A.; Benet-Buchholz, J.; McGrady, J. E.; Maseras, F.; Vilar, R. *J. Am. Chem. Soc.* **2006**, *128*, 6376−6390.

(3) During the preparation of this paper, the following paper was published with the first crystal structure of an oxidative addition complex composed of a biaryl-based ligand (of the type L−Pd(Me)OTf): Yamashita, M.; Takamiya, I.; Jin, K.; Nozaki, K. *J. Organomet. Chem.* **2006**, *691*, 3189−3195.

(4) (a) Huang, X.; Anderson, K. W.; Zim, D.; Jiang, L.; Klapars, A.; Buchwald, S. L. *J. Am. Chem. Soc.* **2003**, *125*, 6653−6655. (b) Nguyen, H. N.; Huang, X.; Buchwald, S. L. *J. Am. Chem. Soc.* **2003**, *125*, 11818−11819.

(5) Frisch, M. J. et al. *Gaussian 03*, Revision B.05; Gaussian, Inc., Wallingford, CT, 2004. See the Supporting Information for the full citation.

(6) (a) Becke, A. D. *J. Chem. Phys.* **1993**, *98*, 5648−5652. (b) Lee, C.; Yang, W.; Parr, R. G. *Phys. Rev. B* **1988**, *37*, 785.

10.1021/om0701017 CCC: $37.00 © 2007 American Chemical Society
Publication on Web 03/27/2007

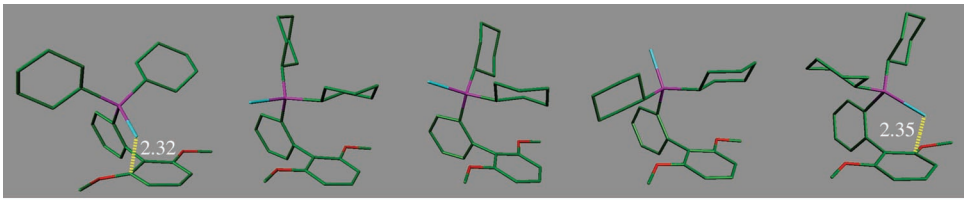

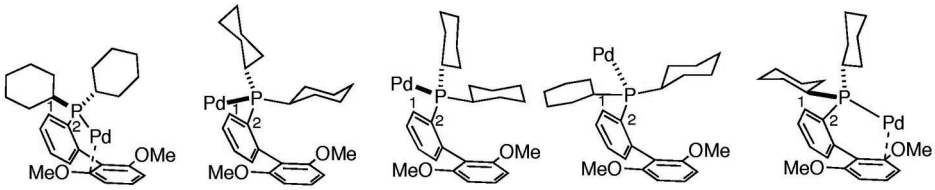

3 **4** **5** **6** **7**

Compound	Rel. E (kcal/mol)[a]	Rel E. (kcal/mol)[b]	Rel E including solvation (kcal/mol)[b,c]	ΔE_{solv} (kcal/mol)[d]
3	**0**	**0**	**0**	-1.6
4	8.8	8.3	7.8	-2.1
5	9.7	9.0	8.5	-2.1
6	3.7	3.9	3.3	-2.2
7	0.9	0.8	0.8	-1.6

[a] At 6-31G/6-31G(d)/LANL2DZ+ECP. [b] At 6-311++G(2d,2p)/LANL2DZ+ECP. [c] In PhMe (ε=2.379), using the CPCM-UAKS method. [d] $\Delta E_{solv} = E_{sol} - E_{gas}$

Figure 1. Five optimized structures based upon **1**·Pd and the relative energies of each: (green) carbon; (red) oxygen; (purple) phosphorus; (turquoise) palladium. Hydrogen atoms are omitted for clarity. Distances are shown in Å.

6-31G(d) basis set was used, and for the Pd center, LANL2DZ+ECP[7] was employed. Single-point energy calculations were conducted using geometries of structures from the 6-31G/6-31G(d)/LANL2DZ+ECP calculations. These calculations employed larger basis sets: 6-311++G(2d,2p) for C, H, O, Cl, and P and LANL2DZ+ECP for Pd. Due to the diffuse functions in the single-point energy calculations, a tight SCF was employed. All calculated structures were verified to be local minima (all positive eigenvalues) for ground-state structures or first-order saddle points (one negative eigenvalue) for transition-state structures by frequency calculations. The unscaled Gibbs free energies were calculated at 298.15 K and 1 atm and based upon ideal gas-phase conditions.

Solvation effects were calculated (at 6-311++G(2d,2p) for C, H, O, Cl, and P and LANL2DZ+ECP for Pd) for all structures on the basis of the geometries from the 6-31G/6-31G(d)/LANL2Z+ECP calculations. The CPCM method[8] in conjunction with the UAKS cavity was used. This method has been recently shown to provide more accurate results for neutral molecules (MAD = 0.88 kcal/mol for a test set of 30 neutral molecules at the B3LYP/6-31+G(d)//B3LYP/6-31+G(d) level of theory) than other method/cavity combinations.[9]

Results and Discussion

Calculated Active Catalysts Based Upon 1·Pd and 2·Pd. Because the structure of a catalyst governs its reactivity, information regarding the structural framework of the active species is important to the development of more efficient catalysts. However, it can be very difficult to obtain spectroscopic or structural data on these types of species, due to their oftentimes highly reactive nature.[10] In order to investigate the active structure in Pd-catalyzed cross-coupling reactions using **1** and **2**, we conducted ground-state optimizations on **1**·Pd and **2**·Pd. These calculations located five rotameric structures (Figure 1) for **1**·Pd. The lowest energy structure (**3**, ∠C1−C2−P−Pd = 163°) possesses an η^1 Pd−arene interaction with the ortho carbon of the non-phosphine-containing ring of the ligand. Interestingly, this differs from the **1**·Pd(dba) experimental X-ray crystal structure[2f] and calculated structure,[2f] in which the Pd−arene interaction resides on the ipso carbon. The origin of this phenomenon is unknown; however, the Pd−arene interaction distances in **3** ($Pd-C_{ortho}$ = 2.32 Å) and the experimental structure of **1**·Pd(dba) ($Pd-C_{ipso}$ = 2.37 Å) are very similar. The second structure (**4**, ∠C1−C2−P−Pd = 79°) was located by rotating the phosphorus atom clockwise. This complex is 8.3 kcal/mol higher in energy than **3**, which is likely due to the naked Pd center as well as steric repulsion between one of the cyclohexyl groups on phosphorus and the non-phosphine-containing ring of the ligand. A third local minimum (**5**, ∠C1−C2−P−Pd = 48°) was found by further clockwise rotation of the phosphorus center. This structure is only slightly higher (0.7 kcal/mol) in energy than **4**. Further rotation of the phosphorus center yields **6** (∠C1−C2−P−Pd = −20°), in which the phosphorus center is rotated nearly 180° relative to complex **3**. Complex **6** is only 3.9 kcal/mol higher in energy than **3**, although the cyclohexyl groups are pushed toward the non-phosphine-containing ring of the ligand. This energy difference is most likely a function of both the Pd−arene interaction and the positioning of the cyclohexyl groups in each rotamer. Finally, the last rotamer (**7**, ∠C1−C2−P−Pd = −157°) is nearly identical with **3** except for the positioning of the cyclohexyl

(7) Hay, P. J.; Wadt, W. R. *J. Chem. Phys.* **1985**, *82*, 299−310.
(8) (a) Klamt, A.; Schüürmann, G. *J. Chem. Soc. Perkin Trans.* **1993**, *2*, 799−805. (b) Andzelm, J.; Kölmel, C.; Klamt, A. *J. Chem. Phys.* **1995**, *103*, 9312−9320.
(9) Takano, Y.; Houk, K. N. *J. Chem. Theory Comput.* **2005**, *1*, 70−77.
(10) Phan, N. T. S.; Van Der Sluys, M.; Jones, C. W. *Adv. Synth. Catal.* **2006**, *348*, 609−679.

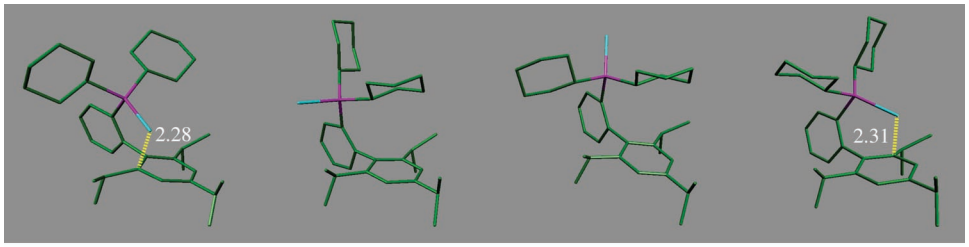

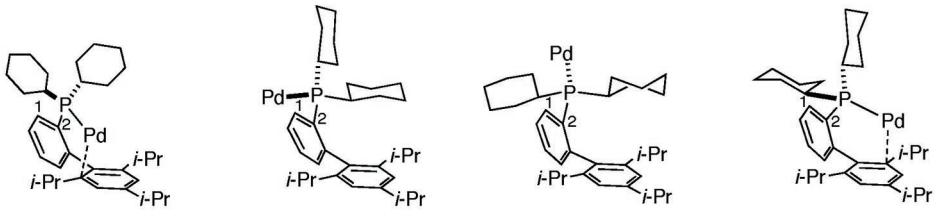

8 **9** **10** **11**

Compound	Rel. E (kcal/mol)[a]	Rel E. (kcal/mol)[b]	Rel E including solvation (kcal/mol)[b,c]	ΔE_{solv} (kcal/mol)[d]
8	0.5	0.5	0.5	-0.8
9	10.4	10.4	9.9	-1.3
10	9.1	9.2	8.6	-1.4
11	**0**	**0**	**0**	-0.8

[a] At 6-31G/6-31G(d)/LANL2DZ+ECP. [b] At 6-311++G(2d,2p)/LANL2DZ+ECP. [c] In PhMe (ε=2.379), using the CPCM-UAKS method. [d] $\Delta E_{solv} = E_{sol} - E_{gas}$

Figure 2. Four optimized structures based upon **2**·Pd and the relative energies of each: (green) carbon; (purple) phosphorus; (turquoise) palladium. Hydrogen atoms are omitted for clarity. Distances are shown in Å.

groups on the phosphorus center, which causes **7** to be 0.8 kcal/mol higher in energy than **3**. Similar to the case for **3**, this confomer possesses a Pd−arene interaction with the ortho carbon of the non-phosphine-containing ring of the ligand (Pd−C_{ortho} = 2.35 Å). It is clear from these structures that the most favored conformations of **1**·Pd are **3** and **7**, with each structure possessing a Pd−arene interaction that likely stabilizes the Pd center prior to the reaction with an aryl halide.

In order to gain a better sense of the solution-state relative energies for each of the structures based upon **1**·Pd, we obtained energies of solvation for each complex in toluene (ϵ = 2.379). Toluene is an attractive solvent, as it is relatively environmentally friendly and can be easily recycled. As such, it has been the solvent of choice for many cross-coupling reactions with (biaryl)phosphine ligands. The solvation energies (Figure 1) were similar in complexes **3**−**7** and ranged from 1.6 kcal/mol for **3** to 2.2 kcal/mol for **6**. Because of the similarity of solvation energies, the overall energy differences between complex **3** and **7** and complexes **4**−**6** decrease only slightly (0.5−0.6 kcal/mol) compared to the differences in their gas-phase values (Figure 1). In order to better approximate solvation effects in **1**·Pd, we included an explicit molecule of toluene in complex **3**. The result of toluene binding the Pd center in complex **3** was the lengthening of the Pd−arene interaction with the non-phosphine-containing ring of the ligand to >3.0 Å with the concurrent generation of a Pd−arene interaction with the toluene molecule (2.31 Å). Although this binding is slightly disfavored (ΔG = +1.8 kcal/mol), it still may play a role in stabilizing the Pd(0) center prior to entrance into the catalytic cycle. However, due to the bulk around the Pd center while bound to toluene, it is likely that dissociation of the toluene molecule is required prior to the formation of an activated complex with an aryl chloride. Upon dissociation of the toluene molecule, re-formation of the Pd−arene interaction may occur with the non-phosphine-containing ring of the ligand, since this is likely extremely rapid due to the intramolecular nature of this interaction. Although a more in-depth analysis of the complexation of explicit solvent molecules to Pd(0) complexes would be highly informative and valuable in determining catalyst stability, a study such as this is beyond the scope of this paper.

Ground-state optimizations on **2**·Pd led to the determination of four local minima (Figure 2). The first local minimum located (**8**, ∠C1−C2−P−Pd = 164°) possesses a geometry similar to that of **3**, albeit with a slightly shorter Pd−C(ortho) interaction (2.28 Å in **8** vs 2.32 Å in **3**). As in **3**, this interaction differs from the X-ray crystal structure of **2**·Pd(dba) by the Pd−arene interaction migrating from the ipso carbon to the ortho carbon of the non-phosphine-containing ring of the ligand. The second local minimum (**9**, ∠C1−C2−P−Pd = 74°) was located by rotation of the phosphorus center clockwise. This isomer allows for one of the cyclohexyl groups on the phosphorus center to sit between the 2′- and 6′-isopropyl groups on the non-phosphine-containing ring of the ligand. However, **9** is disfavored by approximately 10 kcal/mol relative to **8**. Further rotation of the phosphorus center results in complex **10** (∠C1−C2−P−Pd = −32°), which, as in **9**, is disfavored by 9.2 kcal/mol relative to **8**. The final isomer located is the lowest energy structure of **2**·Pd (**11**, ∠C1−C2−P−Pd = −159°) and possesses an η^1 Pd−arene interaction (2.31 Å) with the ortho carbon of the non-phosphine-containing ring of the ligand. It is important to note that, in both **1**·Pd and **2**·Pd, the lowest energy isomers (**3** and **11**, respectively) are those which possess Pd−arene interactions with the non-phosphine-containing ring of the ligand.

The effects of solvation (toluene) were calculated for **2**·Pd at 6-311++G(2d,2p)/LANL2DZ+ECP. For compounds possessing a Pd−arene interaction (**8** and **11**), inclusion of solvent

Chart 1. Potential Energy Surface (PES) Scan Varying the Torsion Angle C1−C2−P−Pd in 1·Pd[a]

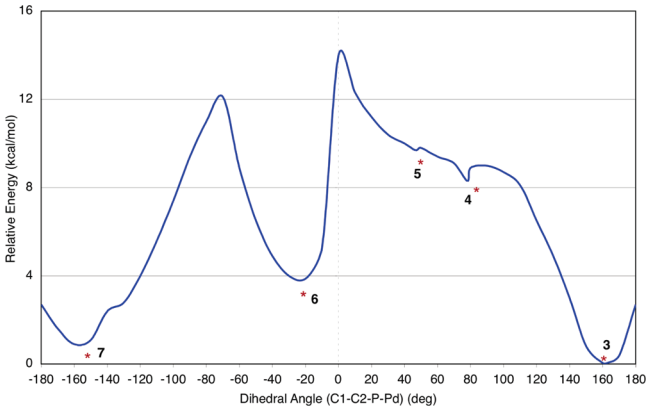

[a] The red asterisks indicate local minima.

Chart 2. Potential Energy Surface (PES) Scan Varying the Torsion Angle C1−C2−P−Pd in 2·Pd[a]

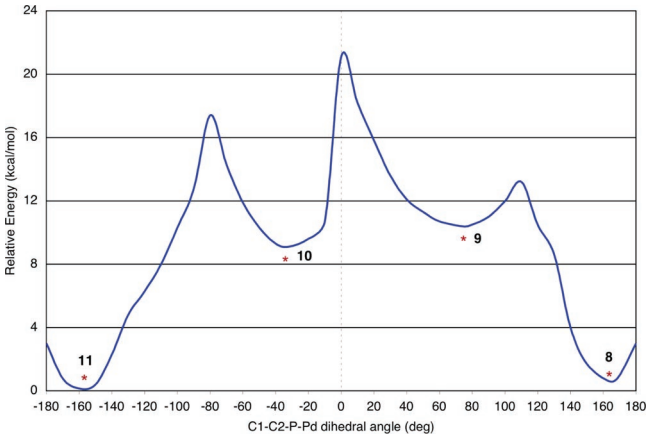

[a] The red asterisks indicate local minima.

lowered their relative energies by 0.8 kcal/mol. Additionally, for the compounds possessing more "exposed" Pd centers (**9** and **10**), solvation impacted the relative energies slightly more: 1.3 and 1.4 kcal/mol, respectively.

Potential Energy Surface of Phosphorus Rotation in 1·Pd and 2·Pd. After locating five local minima of structures based upon **1**·Pd and four local minima of structures based upon **2**·Pd, we next turned our attention to locating transition states for the rotation between these local minima. However, despite numerous attempts, locating rotational transition states (by varying ∠C1−C2−P−Pd) proved to be very difficult. Although several transition states were located, they did not involve bond rotation around C2−P. Due to this difficulty, we concluded that it would be more efficient to conduct a potential energy surface (PES) scan[11] on **1**·Pd and **2**·Pd rather than exert a large amount of computational time on locating rotational transition-state structures. In the PES scan of **1**·Pd, 36 structures were optimized with a constrained C1−C2−P−Pd torsion angle ranging from +180 to −180° (Chart 1). It is apparent that five local minima exist, as found in the previous section, and only two are very similar in energy (**3** and **7**). The highest energy intermediate in our PES scan is that of ∠C1−C2−P−Pd = 0°, which is 14.0 kcal/mol higher in energy than **3**. This structure likely corresponds to the most energetically disfavored transition state for the rotation around C2−P and, therefore, the rate-limiting step for this rotational process. Unfortunately, in attempts to find a transition-state structure with ∠C1−C2−P−Pd = 0°, the located first-order saddle point did not connect the two local minima (**5** and **6)** and instead involved other various rotations of the Pd center. Hence, we approximate $\Delta G^{\ddagger}$ as the global maximum in Chart 1 (14.0 kcal/mol). This relatively low energy value leads us to believe that rotation around C2−P can occur rapidly under typical amination and Suzuki−Miyaura reaction conditions (60−100 °C) and possibly at room temperature, although the highest concentration of **1**·Pd will exist with a Pd−arene interaction (as in **3** and **7**).

The PES scan for **2**·Pd has several features similar to those of **1**·Pd: namely, two local minima that possess Pd−arene interactions (**8** and **11**) (Chart 2). However, the most obvious difference between the two PES scans is the lack of a fifth local minimum for **2**·Pd and, more importantly, the energy of the local maxima (21.1 kcal/mol), which occurs at ∠C1−C2−P−Pd = 0° for **2**·Pd. This value suggests that complete rotation around C2−P is substantially more difficult for **2**·Pd than for **1**·Pd and may be difficult at room temperature. Clearly, as the sizes of the substituents on the 2′- and 6′-positions of the biaryl are increased, steric interactions between these substituents and the cyclohexyl groups on the phosphorus center influence rotation around the C2−P bond. As rotation is kinetically disfavored and other processes with activation energies substantially lower than rotation around the C2−P bond can occur involving **2**·Pd (e.g., oxidative addition; vide infra), the local minima **8** and **11** are likely the only two conformers that contribute to the structure of **2**·Pd. This interaction likely helps stabilize the Pd center from aggregation and decomposition after reductive elimination and prior to oxidative addition.

Attempts To Use Model Systems for Structures Based upon 1·Pd and 2·Pd. The necessity for all-atom calculations for these types of complexes is illustrated in Figure 3. Oftentimes, structures are optimized by substituting a hydrogen atom for an aromatic or alkyl group: e.g., PH_3 is often used in place of PPh_3. In order to evaluate the validity of such an approximation in Pd complexes composed of **1** or **2**, we optimized analogous structures of **3** and **6** (Figure 3, **12** and **13**) and of **8** and **10** (Figure 3, **14** and **15**) in which two hydrogen atoms were substituted for the two cyclohexyl groups on phosphorus.

As illustrated in Figure 3, the results of this comparison demonstrate the perils inherent to such approximations. The lowest energy isomers between the **12**/**13** and **3**/**6** pairs have a combined relative energy difference of 6.2 kcal/mol. More significantly, whereas the lowest energy isomer from the all-atom calculation places the palladium center above the non-phosphine-containing ring of the ligand, **3**, the lowest energy isomer of the approximated structure rotates the palladium center away from the non-phosphine-containing ring of the ligand, **13**. When the same calculations were conducted for **2**·Pd, a similar trend was found. Approximated structures **14** and **15** were found to be nearly identical in energy (**14** is 0.1 kcal/mol higher in energy than **15**). Clearly, this approximation, which maintains some electronic features of the all-atom structures such as the Pd−arene interaction, is inadequate and may lead to inaccurate interpretations. While the all-atom calculations require much more computational cost, they are necessary for this class of ligand complexes to ensure meaningful results. The need to conduct all-atom calculations is not unanticipated for these classes of complexes, as many years of research have been devoted to designing and redesigning (biaryl)phosphine ligands. In the design of (biaryl)phosphine ligands, perturbation of the non-biphenyl substituents of the phosphines has been often

(11) Ziegler, T.; Autschbach, J. *Chem. Rev.* **2005**, *105*, 2695−2722.

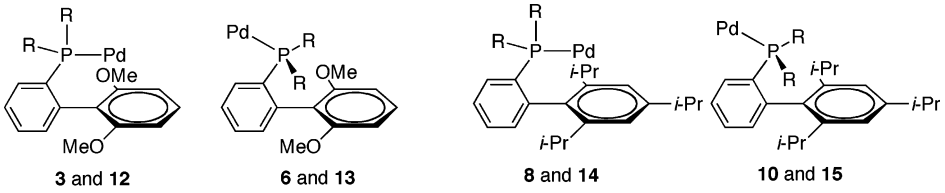

Compound	Rel. E (kcal/mol)[a]
3 R = Cy	0
6 R = Cy	3.9
12 R = H	2.3
13 R = H	0

Compound	Rel. E (kcal/mol)[a]
8 R = Cy	0
10 R = Cy	9.2
14 R = H	0.1
15 R = H	0

[a] Geometries optimized at 6-31G/6-31G(d)/LANL2DZ+ECP; single point energies calculated at 6-311++G(2d,2p)/LANL2DZ+ECP

Figure 3. Structures of **1**·Pd and **2**·Pd replacing the cyclohexyl groups on the phosphorus center with hydrogen atoms.

shown to dramatically affect the reactivity of associated Pd complexes (e.g., biarylPCy$_2$ vs biarylPhP(*t*-Bu)$_2$).[12] Such differences in reactivity would be entirely overlooked using approximations as described above. Thus, we recommend that an all-atom DFT or an ONIOM[13] approach be taken when optimizing structures and calculating thermodynamic and kinetic parameters with (biaryl)phosphine ligands.

Oxidative Addition Complexes. Having explored Pd(0) complexes with **1** as the supporting ligand, the next logical step was to investigate ligated Pd(II) complexes such as oxidative addition species. Despite numerous attempts employing various conditions, we have not been able to obtain structural information on a dialkyl(biaryl)phosphine−Pd oxidative addition complex by X-ray crystallography.[3] Thus, we again turned to DFT calculations in order to gather insight into the structural framework of oxidative addition complexes based upon **1**·Pd. In this case, we located eight possible complexes by performing ground-state energy optimizations on the oxidative addition product of **1**·Pd and chlorobenzene (Figure 4). Two of the eight structures place the Pd center above the ipso carbon of the non-phosphine-containing ring of the ligand and two structures position the Pd away from the non-phosphine-containing ring of the ligand, while the remaining four structures position the Pd near the oxygen atom of the methoxy group. Two of the structures, **16** and **23**, are clearly favored over the others and are identical in energy when using the B3LYP/6-311++G(2d,-2p)/LANL2DZ+ECP level of theory. Complex **16** possesses a Pd−arene interaction with the ipso carbon of the non-phosphine-containing ring of the ligand (2.86 Å), while **23** possesses a Pd−O interaction with an oxygen atom of the methoxy group on the non-phosphine-containing ring of the ligand (2.30 Å). Both of these structures have the chloride atom trans to the phosphine atom. When the chloride and phenyl groups of **16** are interchanged, the resulting structure, **17**, is 9.7 kcal/mol higher in energy, although a shorter Pd−arene interaction is present (2.52 Å). This large increase in energy most likely results from the large trans influence of the phosphine.[14] The trans orientation of the phosphine and halide are consistent with X-ray crystal structures of various monoligated Pd(aryl)X species.[3,15] Two other local mimima composed of **1**·Pd(Ph)Cl, **18** and **19**, were located in which the Pd center points away from the non-phosphine-containing ring of the ligand. Structure **18**, with the chloride atom trans to the phosphorus center, is 6.7 kcal/mol higher in energy than **16** and **23**, while structure **19**, with the chloride cis to the phosphorus, is 16.8 kcal/mol higher in energy than **16** and **23**. Again, this difference in energy likely arises from the trans influence, which favors the positioning of the chloride atom trans to the phosphorus atom. The final three structures, **20**−**22**, have the Pd center in close proximity to the oxygen atom of the methoxy group on the non-phosphine-containing ring of the ligand. Complexes **21** and **22** possess a Pd−O interaction (2.33, and 2.22 Å, respectively), although **22** is very disfavored (by 12.8 kcal/mol) since the chloride is cis to the phosphorus, while **21** is only 3.2 kcal/mol higher in energy than **16** and **23**. Similarly, complex **20** is only 2.9 kcal/mol higher in energy than **16** and **23**, although the Pd−O interaction does not exist in this structure (Pd−O distance 3.20 Å).

It is clear from the relative energies of the various isomers **1**·Pd(Ph)Cl that the chloride trans to the phosphorus center rather than cis is much more favored in all complexes. Hence, while examining possible isomers of **2**·Pd(Ph)Cl, we did not attempt to optimize any structures with the chloride cis to the phosphorus center. However, we were able to locate four distinct local minima for **2**·Pd(Ph)Cl (Figure 5). The lowest energy isomer, **24**, is that with the Pd center directly above the non-phosphine-containing ring of the ligand (Pd−C(ipso) distance of 2.88 Å). Rotation of the phosphorus center yields complex **25**, which is 6.9 kcal/mol higher in energy than **24**. This complex is similar in geometry to **21** above but lacks the Pd−oxygen interaction. Further rotation of the phosphorus center leads to complex **26**, which is analogous to **19**, and is disfavored by 8.3 kcal/mol. Finally, the last complex located, **27**, positions the Pd center distal from the non-phosphine-containing ring of the ligand and is energetically similar to **26** (8.2 kcal/mol less favored than **24**). It is clear from the relative energies of the depicted local minima that **2**·Pd(Ph)Cl will mainly exist in a geometry exemplified by complex **24** during a cross-coupling reaction.

The solvation energies of **2**·Pd(Ph)Cl are similar to those of **1**·Pd(Ph)Cl. The isomers without any Pd−arene interactions are most affected by inclusion of PhMe ($\Delta G_{solv} = -4.0$ to -4.2 kcal/mol), while complex **24** gains 3.3 kcal/mol from the

(12) Strieter, E. R.; Blackmond, D. G.; Buchwald, S. L. *J. Am. Chem. Soc.* **2003**, *125*, 13978−13980.
(13) Maseras, F.; Morokuma, K. *J. Comput. Chem.* **1995**, *16*, 1170−1179.
(14) Appleton, T. G.; Clark, H. C.; Manzer, L. E. *Coord. Chem. Rev.* **1973**, *10*, 335−422.
(15) Stambuli, J. P.; Incarvito, C. D.; Buhl, M.; Hartwig. J. F. *J. Am. Chem. Soc.* **2004**, *126*, 1184−1194.

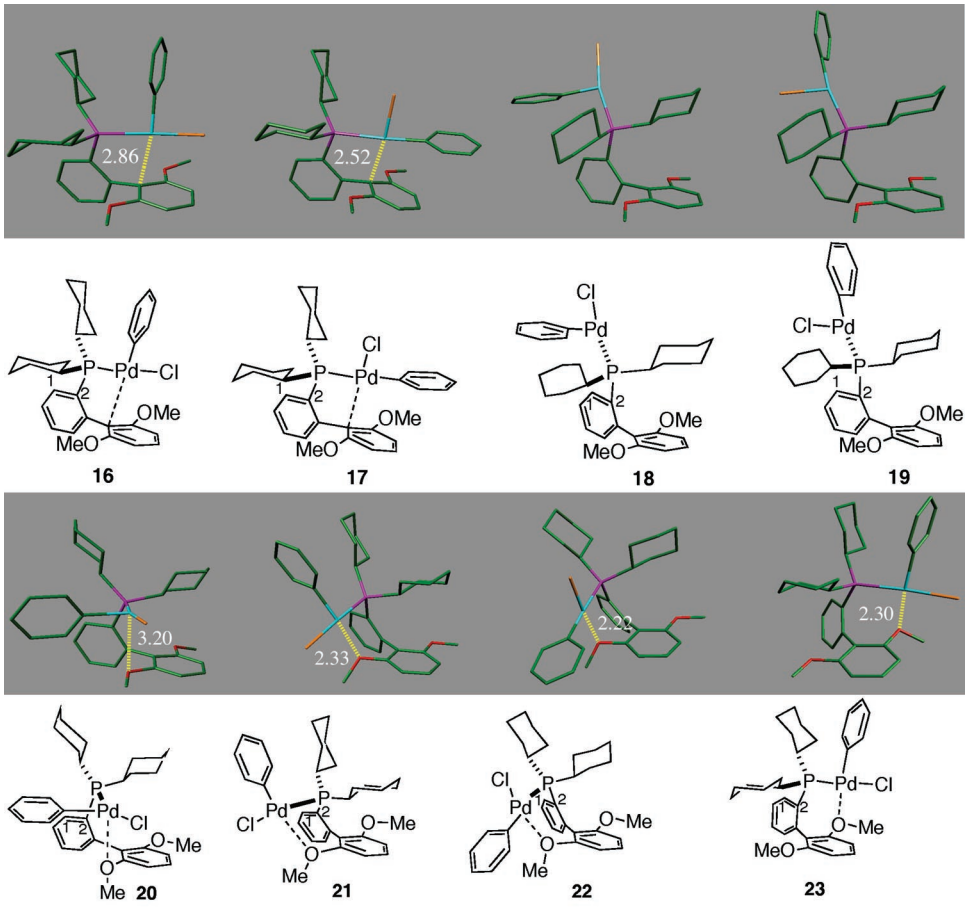

Compound	Rel. E (kcal/mol)[a]	Rel E. (kcal/mol)[b]	Rel E including solvation (kcal/mol)[b,c]	ΔE_{solv} (kcal/mol)[d]
16	3.5	**0**	0.8	-3.9
17	13.6	9.7	10.6	-3.8
18	9.8	6.7	6.7	-4.7
19	20.7	16.8	18.2	-3.3
20	5.3	2.8	3.7	-3.8
21	2.7	3.2	3.2	-4.7
22	12.3	12.8	13.8	-3.7
23	**0**	**0**	**0**	-4.7

[a] At 6-31G/6-31G(d)/LANL2DZ+ECP. [b] At 6-311++G(2d,2p)/LANL2DZ+ECP. [c] In PhMe (ε=2.379), using the CPCM-UAKS method. [d] $\Delta E_{solv} = E_{sol} - E_{gas}$

Figure 4. Eight optimized oxidation addition complexes composed of **1**·Pd(Ph)Cl and the relative energies of each isomer.

inclusion of PhMe. Regardless of this difference, complex **24** is still favored by 6.2 to 7.5 kcal/mol over the other three isomers.

From the data regarding **1**·Pd(Ph)Cl, it is clear that two complexes, **16** and **23**, are both likely to exist in a given Pd-catalyzed cross-coupling reaction prior to amine binding or transmetalation. We believe that the ability of **1** to stabilize the Pd(II) center of oxidative addition complexes through labile Pd−arene and Pd−O interactions is partially responsible for the effectiveness of **1** as a supporting ligand in Pd-catalyzed cross-coupling reactions, particularly the Suzuki−Miyaura coupling reaction. The existence of the extra interaction in complex **23** (Pd−O interaction) relative to **2**·Pd(Ph)Cl (where only the Pd−C(ipso) interaction exists) likely further stabilizes the oxidative addition complex prior to transmetalation of the boronic acid, which is most likely the rate-limiting step in the catalytic cycle. It may be that the extra stability imparted by **1** is not required in amination reactions (in which **2** is most often the superior ligand), as amine binding is much more rapid than transmetalation. However, with both **1** and **2**, the greater the ability of the ligand to stabilize the Pd center in oxidative addition complexes, the less readily catalyst decomposition will occur at that state in the catalytic cycle.

NMR Analyses of 1·Pd(Ph)Cl. As stated previously, we have been unable to obtain any crystallographic structural information on a monoligated Pd(Ph)X species. However, we have successfully prepared the oxidative addition product of **1**·Pd and chlorobenzene.[16] An analogous oxidative addition complex was also prepared using 2-dicyclohexylphosphino-2,6′-diethylbiphenyl (**28**), which is isosteric to **1**. However, unlike **1**·Pd(Ph)Cl, **28**·Pd(Ph)Cl could not be successfully isolated and was

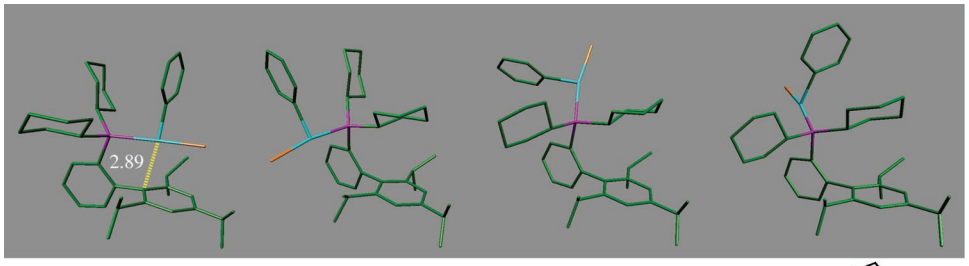

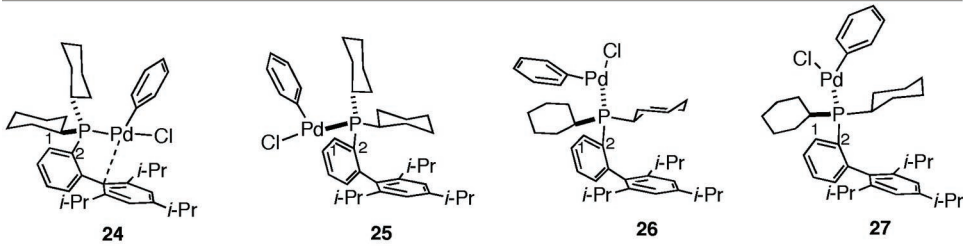

Compound	Rel. E (kcal/mol)[a]	Rel E. (kcal/mol)[b]	Rel E including solvation (kcal/mol)[b,c]	ΔE_{solv} (kcal/mol)[d]
24	**0**	**0**	**0**	-3.3
25	6.8	6.9	6.2	-4.0
26	8.1	8.3	7.5	-4.1
27	8.0	8.2	7.2	-4.2

[a] At 6-31G/6-31G(d)/LANL2DZ+ECP. [b] At 6-311++G(2d,2p)/LANL2DZ+ECP. [c] In PhMe (ε=2.379), using the CPCM-UAKS method. [d] $\Delta E_{solv} = E_{sol} - E_{gas}$

Figure 5. Four optimized oxidation addition complexes composed of **2**·Pd(Ph)Cl and the relative energies of each isomer.

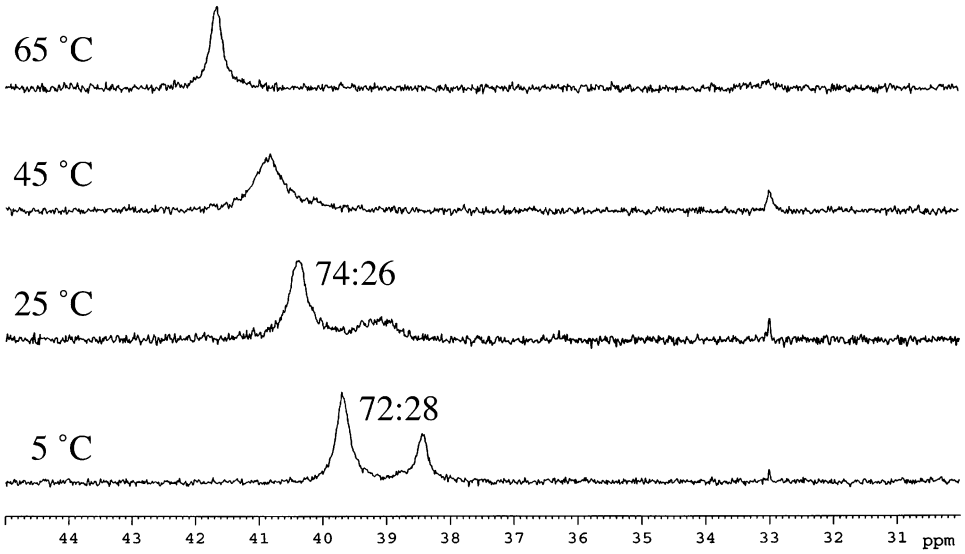

Figure 6. ^{31}P NMR spectra of **1**·Pd(Ph)Cl at various temperatures.

prepared in situ (see the Supporting Information). Figure 6 contains ^{31}P NMR spectra, in toluene, of **1**·Pd(Ph)Cl at various temperatures (5, 25, 45, and 65 °C). At 25 °C, three distinct peaks appear in the ^{31}P NMR spectrum with a relative ratio of 72:25:3. Disregarding the minor peak (assigned as the μ-chloride dimer based upon the solution and solid-state structure of **1**·Pd(Ph)Cl in CH_2Cl_2[16,17]), the ratio of the two major peaks is 74:26, or approximately 3:1. We believe that these two peaks correspond to the two lowest energy rotamers of **1**·Pd(Ph)Cl, **16** and **23**, as calculated above. The 3:1 ratio of the two major peaks translates into $\Delta G_{294} = 0.64$ kcal/mol for **16**/**23**, which is in excellent agreement with the solvent-included 6-311++G-(2d,2p)/LANL2DZ+ECP calculation of 0.8 kcal/mol (ΔE_{solv}-(**16**−**23**)). When the NMR sample of **1**·Pd(Ph)Cl is heated, the two peaks rapidly and reversibly coalesce such that separation is nearly undetectable at 45 °C. Hence the barrier of interconversion

(16) We obtained an X-ray crystal structure of an oxidative addition complex composed of **1** and PhCl from CH_2Cl_2; however, on the basis of the ^{31}P NMR chemical shift, the species likely exists as a μ-Cl dimer in CH_2Cl_2 and indeed exists as a dimer in the solid state (when crystallized from CH_2Cl_2). The NMR spectra in Figure 6 were measured in toluene, a common solvent for cross-coupling processes, and **1**·Pd(Ph)Cl exists predominantly as two monomeric species. See the Supporting Information for details.

(17) Widenhoefer, R. A.; Buchwald, S. L. *Organometallics* **1996**, *15*, 2755−2763.

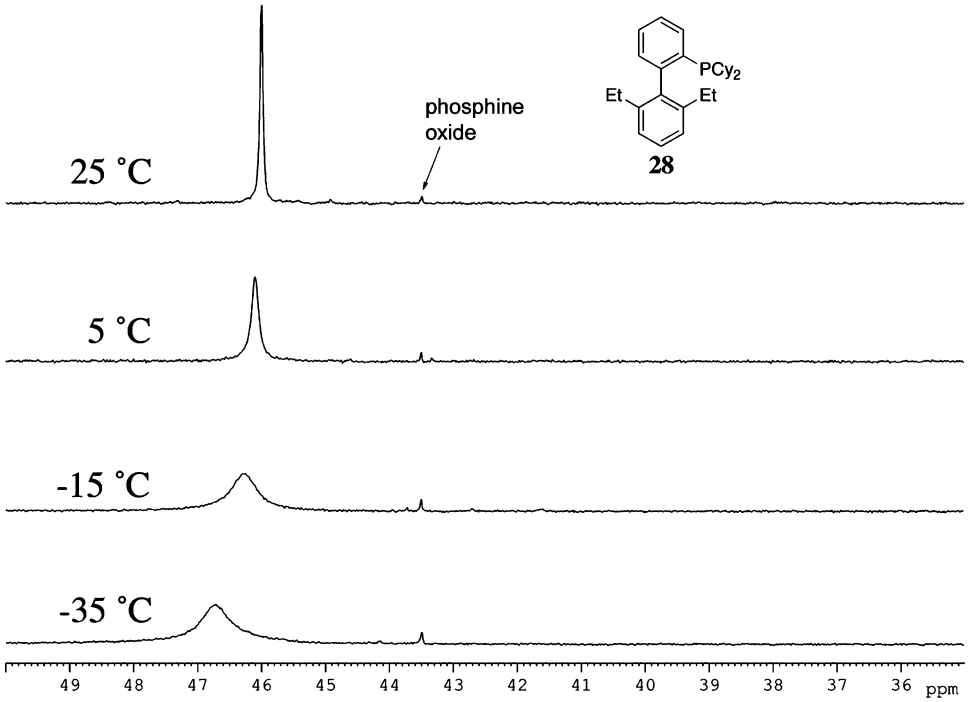

Figure 7. ^{31}P NMR spectra of **28**·Pd(Ph)Cl at various temperatures.

Table 1. Gibbs Free Energy Values for the Reaction of 3 with PhCl

complex	ΔG_{298} (kcal/mol)[a]	complex	ΔG_{298} (kcal/mol)[a]
16	−10.3	**20**	−8.1
17	−1.1	**21**	−10.9
18	−6.5	**22**	−1.8
19	+2.5	**23**	−12.7

[a] For the reaction of **1**·Pd with PhCl, calculated at the 6-31G/6-31G(d)/LANL2DZ+ECP level.

between the two species (which likely corresponds to the barrier of rotation between **16** and **23**) is small.

When the nearly isosteric ligand **28** is substituted for ligand **1**, there no longer exists a functional group on the non-phosphine-containing ring of the ligand that is capable of binding to the Pd(II) center. Accordingly, the ^{31}P NMR spectrum contains only one peak that we attribute to an ipso-bound Pd−arene structure analogous to **16**. When the temperature is lowered from 25 to −35 °C, a single signal remains (Figure 7). The lack of a second species in the ^{31}P NMR spectrum of **28**·Pd(Ph)Cl suggests that one of the peaks in the spectrum of **1**·Pd(Ph)Cl corresponds to **23** (the complex possessing the Pd−O interaction), since the ligands are nearly isosteric. Unfortunately, additional data could not be extracted from the ^{1}H and ^{13}C NMR spectra of **1**·Pd(Ph)Cl and **28**·Pd(Ph)Cl, since they are difficult to interpret due to broad and/or overlapping peaks.

Thermodynamic and Kinetic Parameters of Oxidative Addition. While Figures 4 and 5 illustrate the relative thermodynamic stability of each oxidative addition product, they do not provide insight into the thermodynamic or kinetic parameters of oxidative addition of chlorobenzene to **1**·Pd and **2**·Pd. Therefore, these were investigated for each of the calculated oxidative addition structures. Interestingly, oxidative addition of PhCl to **3** is exergonic for nearly all eight isomers depicted in Figure 4 (Table 1). This large exergonicity likely results from the combination of 1) a highly reactive, yet stable (toward decomposition) **1**·Pd complex, which possesses higher reactivity relative to other active catalysts and 2) the stabilization of the oxidative addition product by way of Pd-arene and/or Pd−O interactions (for **16** and **23**).

Table 2. Gibbs Free Energy Values for the Reaction of 11 with PhCl

complex	ΔG_{298} (kcal/mol)[a]	complex	ΔG_{298} (kcal/mol)[a]
24	−6.9	**26**	+0.5
25	−1.5	**27**	−0.5

[a] For the reaction of **2**·Pd with PhCl, calculated at the 6-31G/6-31G(d)/LANL2DZ+ECP level.

The thermodynamic parameters for oxidative addition to **2**·Pd (Table 2) follow a slightly different trend to those to **1**·Pd, i.e., the exergonicity for each reaction in Table 2 is less negative than that for the respective exergonicity in Table 1. For example, ΔG_{298} for the lowest energy species of **2**·Pd(Ph)Cl (−6.9 kcal/mol) is 4 kcal/mol greater than the lowest energy isomer of **1**·Pd(Ph)Cl (−10.9 kcal/mol). This difference may be from the difference in stability of **1**·Pd vs **2**·Pd; namely, that **2**·Pd is more stable than **1**·Pd. This may be due to a more favorable interaction between the Pd center and the non-phosphine-containing ring of **2**, as this aromatic ring is less electron-rich than the non-phosphine-containing ring in **1** and may bind more effectively to Pd(0). Additionally, the oxidative addition complexes composed of **2** do not have the opportunity to be stabilized by a Pd−O interaction as with **1**. Studies are underway to determine the strength of Pd−arene and Pd−O interactions in monoligated Pd(0) and Pd(II) complexes composed of (biaryl)phosphine ligands.

The kinetic barriers for oxidative addition of PhCl to **1**·Pd and **2**·Pd were also explored. Figures 8 and 9 contains transition-state structures for oxidative addition of chlorobenzene to the most stable isomer of **1**·Pd (compound **3**) and the most stable isomer of **2**·Pd (compound **11**). It was found that the Pd−arene interaction greatly lengthens (to 3.49 Å in **29** and 3.33 Å in **30**) upon formation of an activated complex composed of PhCl and **1**·Pd. This suggests that the Pd−arene interaction in **3** does not increase the electron density on the Pd center during oxidative addition and that Pd−arene interactions only stabilize the Pd center in the ground-state structures of **1**·Pd and **1**·Pd-

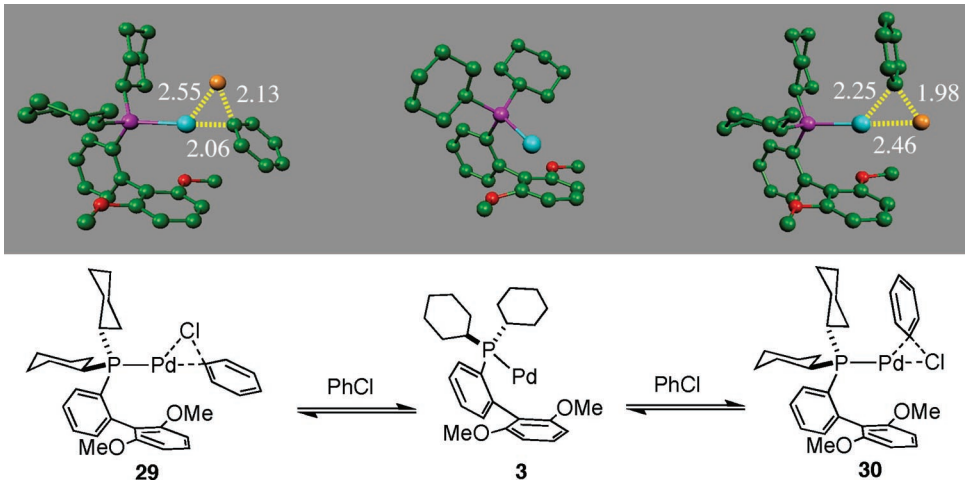

Figure 8. Two transition-state structures of **1**·Pd and chlorobenzene leading to oxidative addition products based upon **1**·Pd(Ph)Cl.

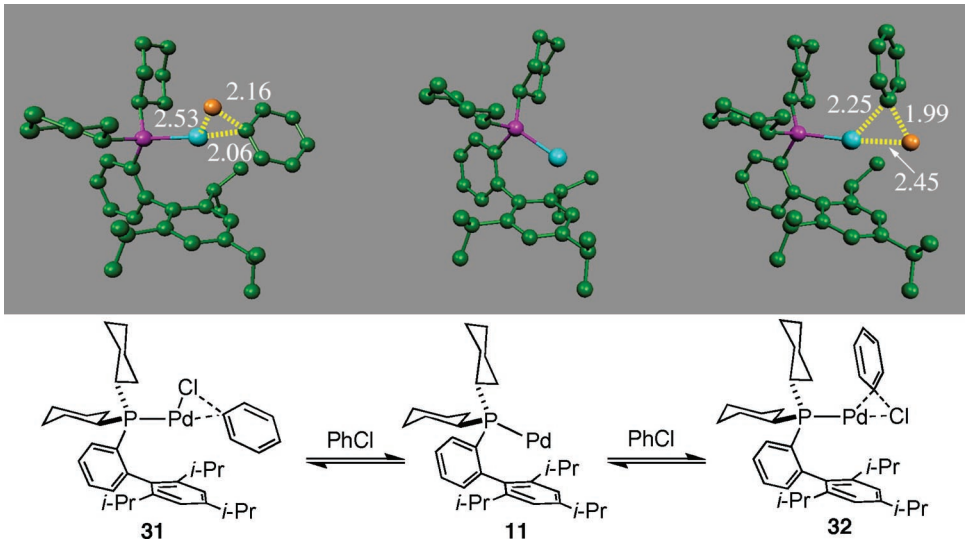

Figure 9. Two transition-state structures of **2**·Pd and chlorobenzene leading to oxidative addition products based upon **2**·Pd(Ph)Cl.

(Ph)Cl. The $\Delta G^{\ddagger}$ values for **29** and **30** are 11.6 and 12.3 kcal/mol, respectively. Similar transition-state structures were located for the reaction of chlorobenzene with the lowest energy isomer of **2**·Pd (complex **8**). The Pd−arene interaction in **2**·Pd lengthens to 3.64 Å for **31** and 3.26 Å for **32** upon formation of an activated complex consisting of **2**·Pd and PhCl. In comparison to the activation energies of oxidative addition transition-state structures with **1**, the $\Delta G^{\ddagger}$ values for **31** and **32** are slightly larger: 14.8 and 13.4 kcal/mol, respectively. Although these values are slightly higher, the $\Delta G^{\ddagger}$ values for the reaction of PhCl with both **1**·Pd and **2**·Pd suggest that oxidative addition can proceed at room temperature. This hypothesis is supported by NMR experiments that show the ability of even hindered aryl chlorides (e.g., 2-chlorotoluene) to oxidatively add to catalysts based upon **1**·Pd at temperatures as low as 0 °C and to catalysts based upon **2**·Pd at room temperature.[18] The $\Delta G^{\ddagger}$ values also suggest that oxidative addition is not the turnover-limiting step in Pd-catalyzed cross-coupling reactions and is quite facile once a monoligated Pd species is formed. Finally, although the activation energies for oxidative addition of PhCl to **1**·Pd (**29** and **30**) and for oxidative addition of PhCl to **2**·Pd (**31** and **32**) are both similar, the only favored oxidative addition isomers are that with the chloride trans to the phosphorus center (corresponding to transition-state structures **30** and **32**).

In conclusion, we have used DFT to locate possible active catalysts based upon **1**·Pd (five isomers) and **2**·Pd (four isomers), several oxidative addition products of PhCl to **1**·Pd and **2**·Pd, and transition state structures of PhCl reacting with **1**·Pd and **2**·Pd using an *all-atom* DFT approach. The use of an *all-atom* DFT approach instead of commonly used approximations (i.e., substituting H for alkyl or aryl groups on the phosphorus center) was found to be of importance, as vastly different energy values were obtained for approximated calculations versus all-atom calculations. Pd−arene or Pd−O (in the case of **1**) interactions were present in all energetically favored complexes consisting of Pd(0) and Pd(II) bound to **1** and **2**. We believe that these interactions are one of the main reasons for the stability of Pd complexes derived from these ligands. Although these interactions impart stability in intermediates, i.e., the active catalyst and oxidative addition structures, they are not present in transition state structures, which suggests that the interactions stabilize the catalyst when the Pd is not involved in a step within the catalytic cycle. Additionally, calculated kinetic parameters of oxidative addition of aryl chlorides to **1**·Pd or **2**·Pd strongly suggest that oxidative addition is facile when using **1** or **2** as the supporting ligand for Pd-catalyzed cross-

(18) See the Supporting Information for details.

coupling reactions. Data regarding amine binding to oxidative addition complexes composed of **1** and **2** will be presented shortly.

Acknowledgment. We thank the National Institutes of Health (NIH) for support (No. GM-46059). We thank Merck, Amgen, and Boehringer Ingelheim for additional unrestricted support. T.E.B. was supported, in part, by an ACS Organic Division Award (sponsored by Novartis Pharmaceuticals), which he gratefully acknowledges. M.R.B. thanks the NIH for a postdoctoral fellowship (No. GM-75685). We are also indebted to Dr. Ana Minatti for help in preparing the figures for this paper.

Supporting Information Available: Text, figures, and tables giving the full ref 5, additional experimental details, NMR spectra, and Cartesian coordinates and energies for all optimized structures. This material is available free of charge via the Internet at http://pubs.acs.org.

OM0701017